ACS APPLIED NANO MATERIALS

www.acsanm.org

Article

Bioinspired, Non-Enzymatic, Aqueous Synthesis of Size-Tunable CdS Quantum Dots for Sustainable Optoelectronic Applications

Nur Koncuy Ozdemir, Joseph P. Cline, Tsung-Han Wu, Leah C. Spangler, Steven McIntosh, Christopher J. Kiely, and Mark A. Snyder*

Cite This: *ACS Appl. Nano Mater.* 2023, 6, 7668–7678

Read Online

ACCESS | Metrics & More | Article Recommendations | Supporting Information

ABSTRACT: The enzymatic production of hydrogen sulfide (H_2S) from cysteine in various metabolic processes has been exploited as an intrinsically "green" and sustainable mode for the aqueous biomineralization of functional metal sulfide quantum dots (QDs). Yet, the reliance on proteinaceous enzymes tends to limit the efficacy of the synthesis to physiological temperature and pH, with implications for QD functionality, stability, and tunability (*i.e.*, particle size and composition). Inspired by a secondary non-enzymatic biochemical cycle that is responsible for basal H_2S production in mammalian systems, we establish how iron(III)- and vitamin B_6 (pyridoxal phosphate, PLP)-catalyzed decomposition of cysteine can be harnessed for the aqueous synthesis of size-tunable QDs, demonstrated here for CdS, within an expanded temperature, pH, and compositional space. Rates of H_2S production by this non-enzymatic biochemical process are sufficient for the nucleation and growth of CdS QDs within buffered solutions of cadmium acetate. Ultimately, the simplicity, demonstrated robustness, and tunability of the previously unexploited H_2S-producing biochemical cycle help establish its promise as a versatile platform for the benign, sustainable synthesis of an even wider range of functional metal sulfide nanomaterials for optoelectronic applications.

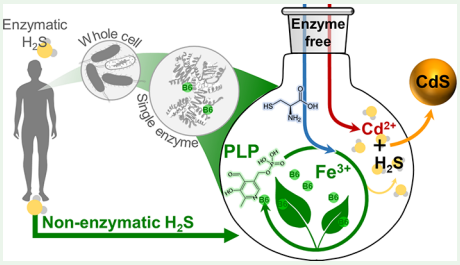

KEYWORDS: *biomineralization, quantum dots, aqueous synthesis, green synthesis, non-enzymatic, low temperature, crystalline nanoparticles*

INTRODUCTION

The identification of sustainable strategies for synthesizing functional nanomaterials has impacted the synthesis of quantum dots (QDs), semiconductor nanomaterials whose unique size- and composition-tunable optical properties make them attractive for optoelectronic applications in photocatalytic H_2 generation, bioimaging, light-emitting devices, solar cells, batteries, and supercapacitors.[1−5] The search for "green" routes to QDs is driven, in part, by the non-sustainable synthesis conditions (*e.g.*, high temperatures and toxic organic solvents) employed for conventional QD synthesis and the costly post-processing (*e.g.*, separations and ligand exchange) required for various applications.[6]

Initiatives aimed at "green" engineering often look to nature for inspiration, with hopes of translating to the laboratory the phenomenal molecular control that biological processes offer under physiological conditions (37 °C, aqueous, and near-neutral pH). In this context, the need for reactive sulfur in the synthesis of metal sulfide QDs has drawn attention to the endogenous production of hydrogen sulfide (H_2S), a bioavailable gas that plays numerous important roles in both physiological and pathological processes.[7−9] The production of H_2S under physiological conditions is known to occur through multiple well-established enzymatic routes.[9,10] Early translation of endogenous enzymatic H_2S production to the low-temperature, aqueous-phase laboratory synthesis of metal sulfide QDs was first demonstrated by leveraging relevant enzymatic pathways in cellular systems.[11−14] Yet, challenges associated with the isolation of the QD products, deriving from their attachment to or uptake by the cells, have led to more recent efforts aimed at harnessing extracellular single enzyme routes for QD biomineralization.

Specifically, we have demonstrated the turnover of the sulfur-containing amino acid, L-cysteine, to H_2S by an engineered strain of cystathionine γ-lyase (CSE) as a single-enzyme platform for the nucleation and growth of functional, size-tunable, and compositionally diverse QDs in buffered solutions of metal salts.[15−21] The activity of CSE for L-cysteine turnover to H_2S derives from the internal Schiff base formed by the docking of vitamin B_6, pyridoxal phosphate cofactor (PLP), to L-lysine residues located in pockets within the apoenzyme (*i.e.*, the complex proteinaceous macromolecular structure). Enzyme activity gradually decays with conversion of

Received: February 21, 2023
Accepted: April 21, 2023
Published: May 2, 2023

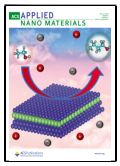

https://doi.org/10.1021/acsanm.3c00805
ACS Appl. Nano Mater. 2023, 6, 7668−7678

the PLP cofactor to thiazolidine upon turnover of the dissolved L-cysteine substrate.[22−24] To this end, we have previously demonstrated how PLP replenishment[24] helps to reform the haloenzyme complex, sustaining CSE activity during cyclic biomineralization of CdS QDs and even offsetting some intrinsic activity loss incurred upon enzyme immobilization.[18]

Despite these advances, the physiological conditions and single-use cofactors required to maximize and sustain enzyme activity and stability restrict the enzymatic QD biomineralization platform. Clear opportunities, therefore, exist for identifying non-enzymatic aqueous biosynthetic routes to H_2S to further advance sustainable QD biomineralization beyond the progress already made by single-enzyme processes[15−21,25,26] over whole-cell approaches.[11−14] Namely, the motivation to avoid the overall enzyme complex (*i.e.*, the haloenzyme or the proteinaceous apoenzyme), but not specifically the separate small molecule cofactor or so-called coenzyme, derives specifically from the sensitivity of the former to temperature- and pH-based denaturation (*i.e.*, loss of critical secondary structure, order, and thus activity), which strictly limits enzymatic synthesis to near-physiological conditions. The concomitant potential to expand viable temperature and pH conditions could additionally help to improve the quality of the all-aqueous QD product and bolster solution stability,[27] respectively. Additionally, elimination of complexation between the rich protein chemistries and synthesis reagents could help circumvent common challenges confounding enzyme-based material synthesis. Yet, while non-enzymatic biochemical routes have been predicted to play an important role in H_2S production in both living and non-living systems, they have remained poorly understood until recently.

As early as the 1970s, work by Gruenwedel and Patnaik,[28] aiming to troubleshoot the occurrence of black deposits in the headspace of canned protein-rich foods,[29] identified the role of metals and PLP in catalyzing high-temperature H_2S liberation from sulfur-containing amino acids under inert (N_2) aqueous conditions. Only recently, however, has the work of Yang and co-workers[25] begun to unravel the mechanistic details of endogenous non-enzymatic production of basal H_2S in mammalian tissues. Such H_2S production shares striking similarities with the exogenous H_2S mechanisms described decades earlier. Specifically, Yang and co-workers have hypothesized a biochemical cycle, summarized in Scheme 1, comprising PLP- and iron (Fe^{3+})-based catalytic liberation of H_2S from sulfur-containing amino acids under low-temperature (4−37 °C) buffered aqueous conditions.[25]

The CSE deactivation chemistry is an integral part of this newly identified biochemical cycle, wherein intermolecular interactions between the free amino group of L-cysteine and the aldehyde group of PLP result in formation of a Schiff base, subsequent cysteine−aldimine complexation, and termination of the reaction with thiazolidine formation. In the presence of Fe^{3+}, however, the biochemical cycle is perpetuated by conversion of the cysteine−aldimine complex instead to a cysteine−quinonoid intermediate upon deprotonation of cysteine. Fe^{3+} then catalyzes thiol elimination, releasing H_2S and forming an aldimine−pyridoxal complex that is hydrolyzed to regenerate PLP, releasing pyruvate and NH_3, and thereby completing and perpetuating the biochemical cycle.

The demonstrated activity of the non-enzymatic H_2S-producing biochemical cycle at temperatures spanning 4 °C[25] to 100 °C[28] indicates its promise for relaxing the tight physiological constraints on temperature, as well as pH and

Scheme 1. Leveraging Cyclic Biochemical H_2S Production from Fe^{3+}, PLP, and Cysteine Chemistry[25] for the Synthesis of CdS Quantum Dots[a]

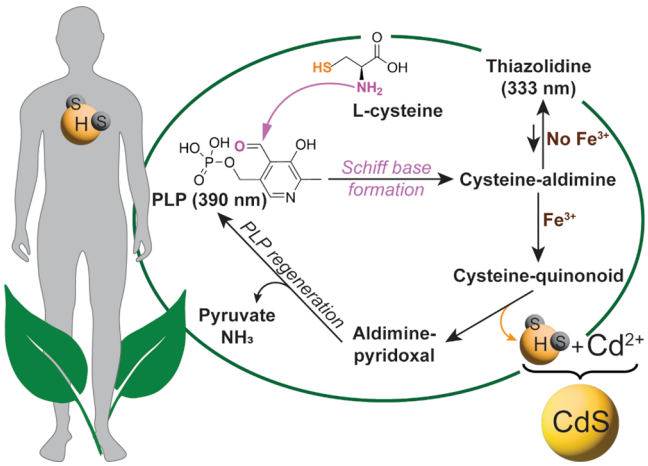

[a]Parenthetical values denote the reference absorption wavelengths of specific compounds.

solution composition, imposed by enzyme-based QD biomineralization. In so doing, this new synthetic route achieves key advances toward principles of "green" engineering, including the multipurposing of reagents, elimination of enzyme and QD purification challenges, exploitation of "green" solvents and abundant reagents, and reduction of the synthetic energy footprint commonly associated with high-temperature QD synthesis. Here, we establish the efficacy of the "green" non-enzymatic PLP- and Fe^{3+}-catalyzed production of H_2S from L-cysteine in the presence of cadmium acetate for CdS QD synthesis (Scheme 1). While Cd itself is not a "green" material, we have employed it here because of the established use of CdS as a literature test bed for QD synthesis. We elucidate the efficacy of the new biosynthetic route for QD synthesis and the impact of pH and temperature on the optical properties of the resulting QDs. We conclude by exploring the robustness and sensitivity of the synthesis to solution composition, underscoring the versatility of the previously unexploited non-enzymatic aqueous route to H_2S for the synthesis of optically tunable QDs that should transcend the CdS test bed employed herein.

EXPERIMENTAL SECTION

Bioinspired, Non-enzymatic, and Aqueous Synthesis of CdS QD Synthesis. Cadmium acetate dihydrate (CdAc; 98%, Alfa Aesar, 100 mM), L-cysteine (Spectrum, 330 mM), pyridoxal 5′-phosphate hydrate (PLP; Sigma, 8 mM), and iron(III) chloride ($FeCl_3$; anhydrous; 98%, Alfa Aesar, 10 mM) stock solutions were prepared in distilled (DI) water. 1× phosphate buffered saline (PBS) was prepared with a composition of 137 mM sodium chloride (NaCl, 99%, Sigma), 2.7 mM potassium chloride (KCl, 99%, Sigma), 10 mM disodium hydrogen phosphate (Na_2HPO_4, 99%, Sigma), and 1.8 mM potassium phosphate monobasic (KH_2PO_4, 99%, Sigma) in DI water, and the pH was adjusted across the maximum buffering range to 7, 7.5, or 8 by dropwise titration of aqueous 1 wt % HCl solution or 1 wt % NaOH solution.

CdS QD synthesis was initiated by the addition of specified concentrations of CdAc and L-cysteine to PBS buffer of specific pH (7, 7.5, or 8.0) followed by the addition of PLP and, subsequently, $FeCl_3$ in solution volumes totaling *ca.* 4 mL. The nominal synthesis solution had a composition of 0.5 mM CdAc, 10 mM L-cysteine, 1 mM PLP, and 10 μM $FeCl_3$ in PBS pH 8 buffer. Samples were sealed

https://doi.org/10.1021/acsanm.3c00805
ACS Appl. Nano Mater. 2023, 6, 7668−7678

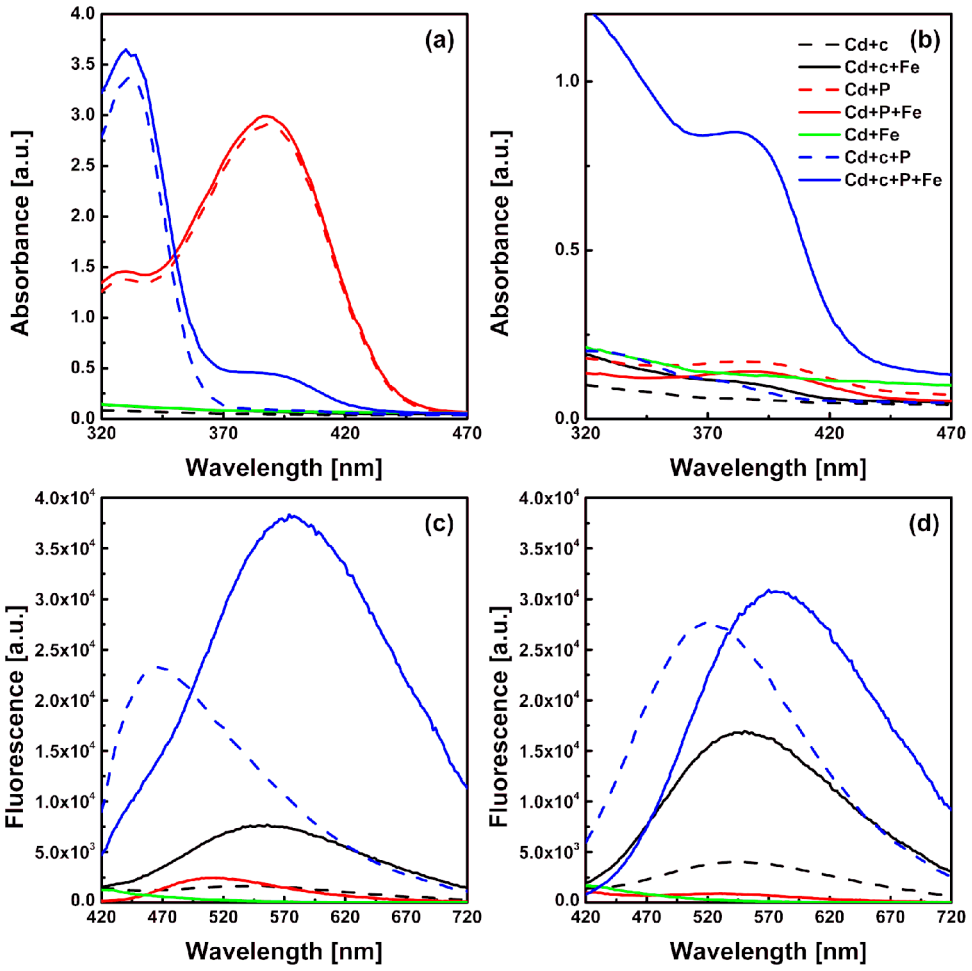

Figure 1. (a, b) Absorbance and (c, d) fluorescence (370 nm excitation) spectra of nominal (a, c) as-synthesized and (b, d) ethanol-washed solutions of 0.5 mM CdAc (Cd), 10 mM cysteine (+c), 1 mM PLP (+P), and/or 10 μM $FeCl_3$ (+Fe) in PBS (pH 8) buffer following incubation at 70 °C for 1 h. Similarly colored dashed and solid spectra indicate the absence or presence of $FeCl_3$, respectively, with all other components included at the same concentrations.

and incubated under dark conditions at specific temperatures (30, 40, 50, or 70 °C). The reaction was quenched through an ethanol-based precipitation−dissolution process,[30] in which 4 volume equivalents (4 V) of 200 proof ethanol was added to a volume, *V*, of the QD synthesis solution followed by centrifugation (10,000 rpm, 15 min), supernatant decantation, QD redispersion in PBS buffer or DI water, and bath sonication (5 min).

Chemical Synthesis of CdS QDs. To understand the effect of H_2S generation rate and concentration on the fluorescence emission peak wavelength of non-enzymatically synthesized CdS QDs, biomineralization was mimicked by room temperature titration of aqueous CdAc solutions with various concentrations of sodium hydrosulfide (NaHS). Specifically, solutions of 0.5 mM CdAc and 10 mM L-cysteine in PBS (pH 8) buffer were separately titrated with either 0.25 mM or 0.50 mM NaHS by stepwise addition of the corresponding NaHS stock solution prepared in DI water. Fluorescence emission measurements were conducted after each titration step.

Lead Sulfide (PbS) Assay for the Determination of the H_2S Generation Rate. Lead sulfide (PbS), resulting from the reaction of lead acetate with H_2S, was employed as a quantitative colorimetric assay of H_2S concentrations and, thereby, generation rates under various synthesis conditions. Solutions of controlled concentrations of H_2S, ranging from 0 to 1 mM, were prepared by decomposition of the same concentration of sodium sulfide hydrate (Na_2S, Alfa Aesar) in PBS pH 8 buffer containing 50 mM L-cysteine (Spectrum). Excess lead(II) acetate trihydrate (ACROS, reagent ACS) was added to each solution at a concentration of 2 mM. The PbS product was detected through its characteristic absorbance band at 500 nm. The resulting colorimetric standard was employed for quantification of time- and temperature-dependent H_2S generation in solutions of nominal composition (10 mM cysteine:1 mM PLP:10 μM $FeCl_3$) in PBS pH 8 buffer. Following incubation at specific temperatures and for specific times, aliquots of the nominal synthesis solution were combined, in equal volumes, with a lead acetate indicator solution (4 mM lead acetate trihydrate, 100 mM L-cysteine in PBS pH 8 buffer). The absorbance intensity at 500 nm was measured and correlated with H_2S concentration through the established calibration.

Assessing Robustness and Versatility of Non-enzymatic Synthesis. The Taguchi orthogonal array approach[31] was employed to identify combinations of three possible concentrations (three-level) of each of four reagents (four-factors), CdAc (0.5, 1.0, and 2.0 mM), cysteine (5, 10, and 20 mM), PLP (0.5, 1.0, and 2.0 mM), and $FeCl_3$ (5, 10, and 20 μM), for assessing the robustness and versatility of the non-enzymatic synthesis of CdS. The Taguchi design with four factors and three levels was completed using the Minitab software, leading to nine solutions with distinct reagent compositions at three different pH (PBS pH 7, 7.5, and 8) conditions.

Characterization. Absorbance and fluorescence (370 nm excitation, 420−720 nm emission wavelengths) measurements were performed on a Tecan Infinite 200 PRO plate reader, using Corning 96-well black plates. Photoluminescence lifetime (PL) measurements were carried out on a Fluorolog-3 spectrofluorometer with an attached Time-Correlated Single-Photon Counting (TCSPC) con-

https://doi.org/10.1021/acsanm.3c00805
ACS Appl. Nano Mater. 2023, 6, 7668−7678

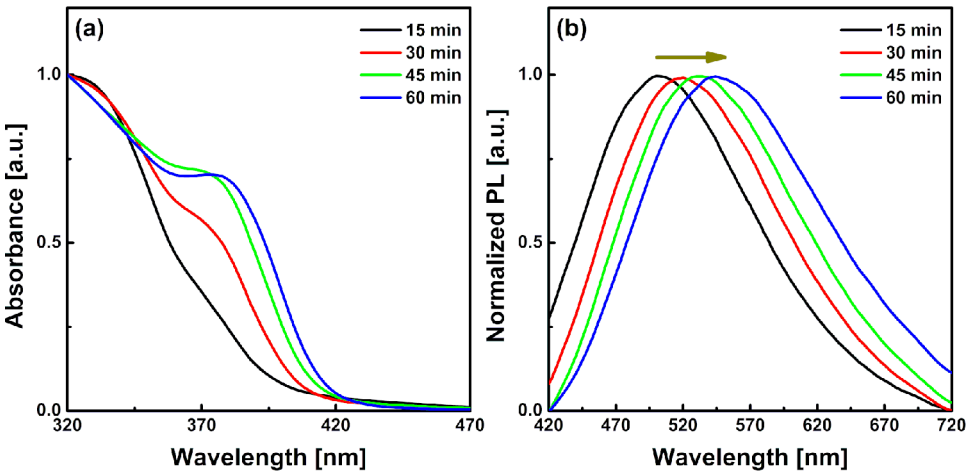

Figure 2. Normalized (a) absorbance and (b) fluorescence (370 nm excitation) spectra of nominal solutions of 0.5 mM CdAc:10 mM cysteine:1 mM PLP:10 μM $FeCl_3$ in PBS (pH 8) buffer following incubation at 70 °C for specified duration and subsequent ethanol wash.

troller using 287 nm excitation (Delta Diode laser) and 530 nm detection. Electron microscopy studies were carried out on QDs that were cleaned by ethanol-induced dissolution−precipitation, re-suspended in DI water, and then dispersed by drop-casting onto holey carbon film (HC400-Cu) transmission electron microscope (TEM) grids. Analysis was conducted on an aberration-corrected JEOL ARM200CF scanning transmission electron microscope (STEM) operating at an accelerating voltage of 200 kV. To determine the particle size distribution (PSD) and polymorphic form of the particles, bright-field and high-angle annular dark field (HAADF) images were collected. Image filtering and analysis were conducted in Digital Micrograph, and JEMS software was used to simulate the crystal structures and diffraction patterns.

RESULTS AND DISCUSSION

To assess the potential for exploiting non-enzymatic biochemical production of H_2S for the aqueous synthesis of CdS QDs, we have studied nominal synthesis compositions employing cysteine (10 mM) and cadmium (0.5 mM) precursor concentrations consistent with earlier enzymatic CdS QD biomineralization studies.[16,19,32,33] Additionally, we have adopted PLP (1 mM) and iron catalyst ($FeCl_3$, 10 μM) compositions that have been demonstrated to yield H_2S under physiological conditions.[25] While much higher concentrations of $FeCl_3$ (1 mM) have been reported separately for H_2S release under nitrogen at elevated temperatures (100 °C),[28] here we have utilized the lowest reported $FeCl_3$ concentrations in an effort to avoid Fe−S cluster formation.

Photoluminescent Particles from Non-enzymatic, Biochemically Produced H_2S. Figure 1a,c shows the UV−vis absorbance and photoluminescence spectra, respectively, following the incubation of CdAc (Cd) in PBS pH 8 buffer at 70 °C for 1 h in the presence of the three reagents comprising the non-enzymatic biochemical H_2S production cycle (Scheme 1)—cysteine (c), PLP (P), and $FeCl_3$ (Fe). Under these conditions (Cd + c + P + Fe), a distinct absorbance band at *ca.* 390 nm and strong photoluminescence are measured, consistent with the successful synthesis of CdS QDs. Whereas CdAc alone undergoes negligible absorbance (not shown), its incubation in the presence of just PLP (Cd + P) also yields a distinct absorbance band at *ca.* 390 nm owing to strong PLP absorbance at this wavelength. Therefore, for insights into the chemistry of CdAc within the H_2S biochemical cycle and for corroboration of its successful exploitation for CdS synthesis, we compared the incubation of various combinations of the cycle components (PLP, L-cysteine, and Fe^{3+}) with CdAc. The identically colored spectra in Figure 1 correspond to comparable synthesis compositions prepared with and without Fe^{3+} and are represented by solid and dashed lines, respectively.

The addition of L-cysteine to PLP and CdAc (Cd + c + P) leads to a shift in the absorbance band to *ca.* 330 nm and the onset of measurable photoluminescence (Figure 1c). This shift in absorbance is consistent with the formation of a Schiff base and subsequent cysteine−aldimine complex[25,34] (Scheme 1). It further reveals the important role of Fe^{3+} in development of the absorbance band at *ca.* 390 nm (Figure 1a) for the nominal synthesis solution (Cd + c + P + Fe). While this band could be attributed to a shift in equilibrium back toward free PLP upon addition of Fe^{3+}, the persistence of the Schiff base (*i.e.*, band at *ca.* 330 nm) and the simultaneous emergence of the strong photoluminescence (Figure 1c) suggest that the non-enzymatic synthesis of CdS QDs is a more likely interpretation. Indeed, the presence of Fe^{3+} in the various solutions studied here has a marked impact only in the case where all three components of the non-enzymatic H_2S-generating biochemical cycle are present (*i.e.*, CdAc, cysteine, and PLP; Cd + c + P + Fe).

The successful production of CdS QDs from the full non-enzymatic biochemical cycle is further clarified when the influence of excess reagents on optical measurements is accounted for, including PLP−cysteine−particle complexation, which has been shown to quench and blue-shift the fluorescence of conjugated particles.[35−38] Upon precipitation−dissolution-based cleaning of the particulate product, strong absorbance (Figure 1b), and thus likely significant particle concentration, is only detected in the case of the full non-enzymatic H_2S chemistry (Scheme 1). Photoluminescence of the cleaned products (Figure 1d) does reveal the formation of fluorescing particles in a subset of the solutions, even in the absence of one or more of the four components of the H_2S-producing biochemical cycle (*e.g.*, Cd + c + P, Cd + c + Fe, and Cd + P + Fe). However, fluorescence is not a direct indicator of particle concentration owing to confounding fluorescence quenching deriving from PLP−cysteine−particle complexation and potential concentration-induced inner filter effects. Instead, Beer−Lambert analysis[39] of the absorbance spectra in Figure 1b (Table S1) shows that particle concentrations

https://doi.org/10.1021/acsanm.3c00805
ACS Appl. Nano Mater. 2023, 6, 7668−7678

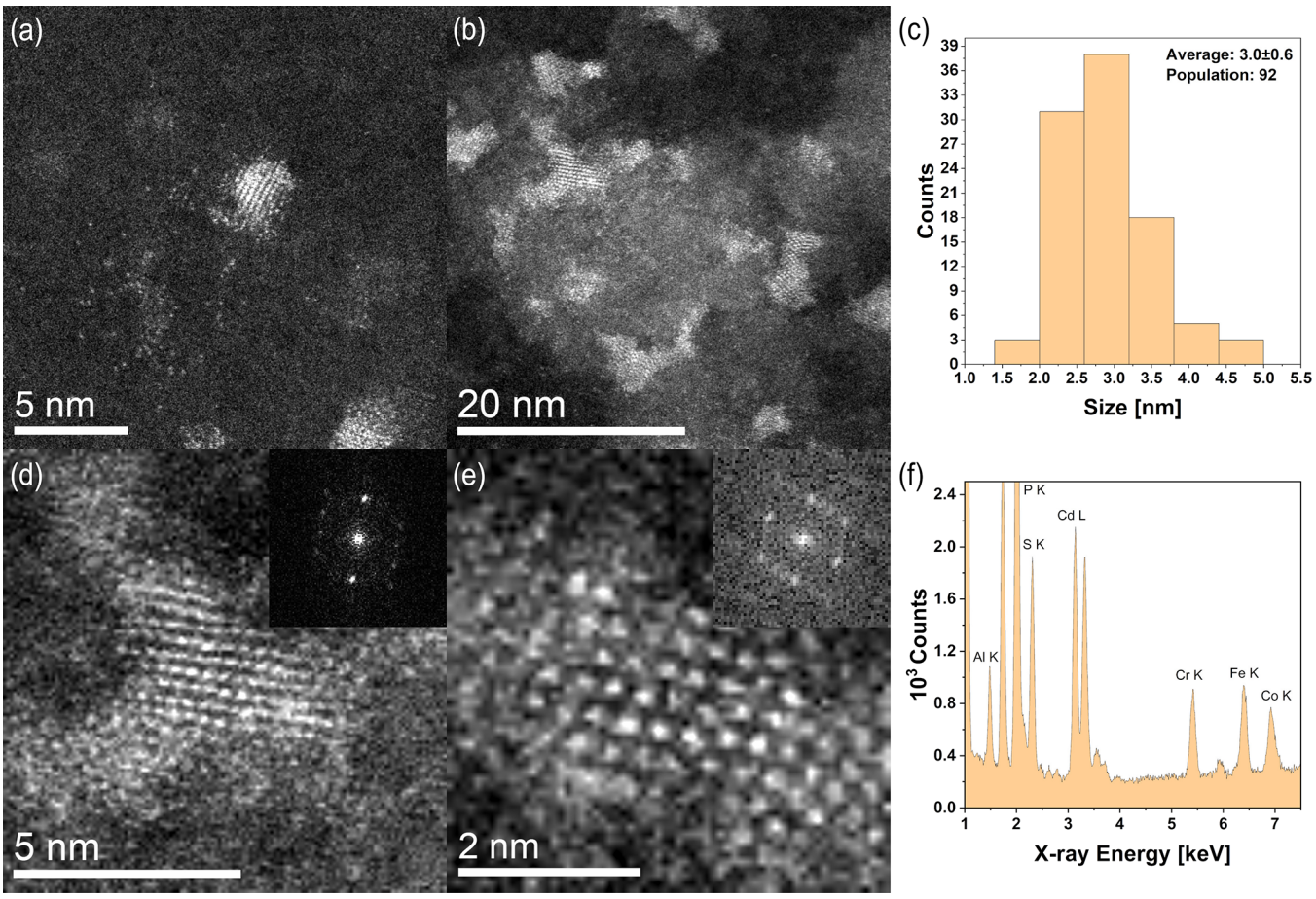

Figure 3. Representative HAADF-STEM images of CdS particles synthesized from nominal solutions of 0.5 mM CdAc:10 mM cysteine:1 mM PLP:10 μM $FeCl_3$ in PBS (pH 8) buffer following incubation at 70 °C for (a) 15 min and (b) 60 min; (c) particle size distribution of the CdS sample incubated for 60 min; CdS; higher magnification HAADF images of individual CdS particles with inset FFTs that match the (d) [100] wurtzite-type and (e) [101] zinc blende-type zone axes of CdS, respectively, as indexed in Tables S3 and S4, respectively; and (f) XEDS spectrum of the CdS agglomerate.

resulting from the full H_2S biochemistry are 7- to more than 34-fold higher than from syntheses that do not contain both PLP and Fe^{3+} (*e.g.*, Cd + c + P, Cd + c + Fe, and Cd + c), establishing the nominal composition employed herein for studying the sensitivity, robustness, and tunability of the biochemical cycle for QD synthesis.

The difference in particle concentration and fluorescence wavelength among the various solution compositions is most likely a manifestation of corresponding differences in the rates of H_2S generation. Namely, higher rates of H_2S production in solutions of CdAc and cysteine have been shown to result in more rapid particle growth, and thus larger particles for a fixed incubation time (Figure S1 and ref 21). The rate of H_2S production, as determined by a lead sulfide (PbS)-based colorimetric assay (Table S2), is highest in the solution containing all components of the non-enzymatic H_2S biochemical cycle (0.242 ± 0.003 mM/h), consistent with the highest measured particle concentrations and largest particle size (*i.e.*, most red-shifted fluorescence) for that composition. This non-enzymatic H_2S generation rate, measured at 70 °C, matches the characteristic rate in enzymatic biomineralization[21] and exceeds by *ca.* 7 times the rate in cysteine−$FeCl_3$ solutions and by more than an order of magnitude the rates measured in cysteine−PLP as well as cysteine-only solutions.

CdS QD Particle Growth, Microstructure, and Morphology. Figure 2 offers insights into the kinetics of particle growth under the nominal synthesis conditions studied here. The time-dependent absorbance and emission spectra reveal the onset of particles within the first 15 min, with a corresponding photoluminescence peak at a wavelength of *ca.* 500 nm. Systematic particle growth, as indicated by the sequential red shifting of the fluorescence spectra by *ca.* 50 nm over the course of 1 h incubation, highlights how incubation time can be leveraged as a simple handle for tuning particle size and thereby optical properties. Similar tunability of particle size with incubation time at *ca.* 20−50% slower rate has been reported[21] for CdS synthesized through enzymatic biomineralization, likely owing to the effect of the lower temperature in the case of the latter on the rate of particle growth.

Particle instability, indicated by visible precipitation, is eventually observed after incubation at 70 °C for *ca.* 90 min, which we attribute to the combined depletion of capping reagent (*i.e.*, L-cysteine) and the formation of less-soluble bulk CdS.[40] However, prior to reaching the point of destabilization, an ethanol wash can be used to quench cysteine turnover and thus halt depletion of the capping cysteine. Subsequent redispersion of the particles in PBS pH 8 buffer and storage at 4 °C leads to extended particle stability as evidenced by the

https://doi.org/10.1021/acsanm.3c00805
ACS Appl. Nano Mater. 2023, 6, 7668−7678

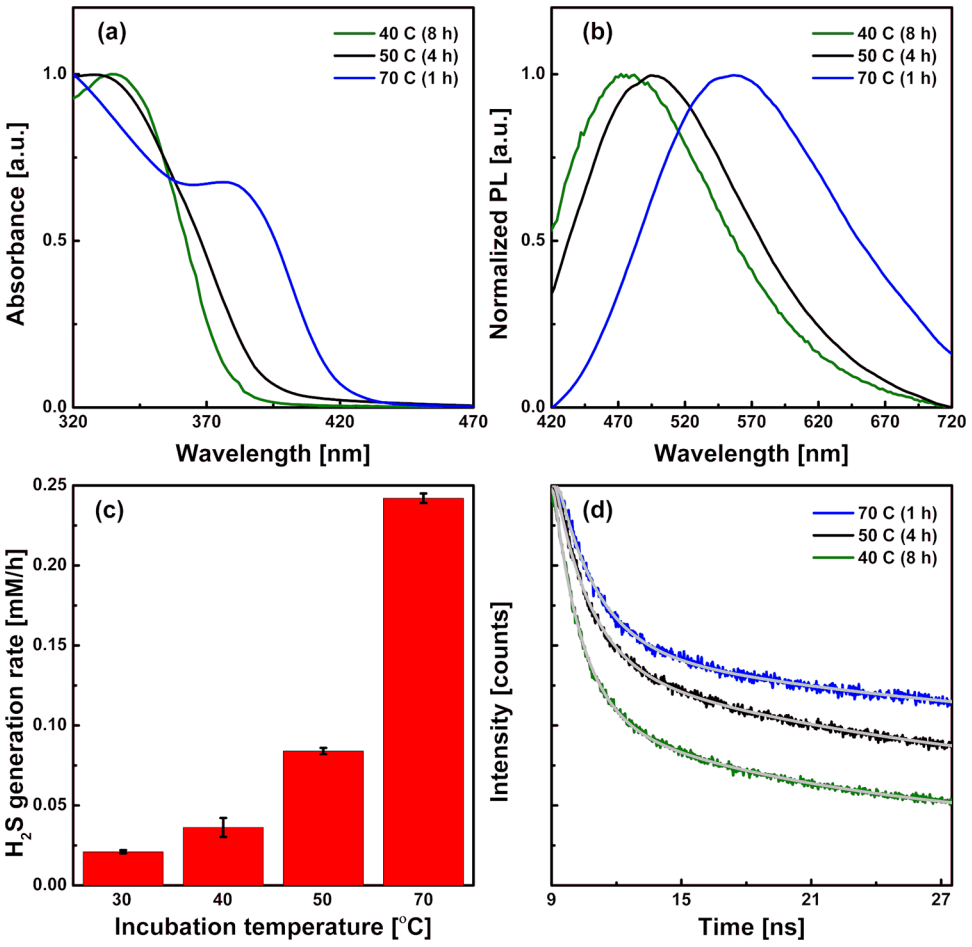

Figure 4. Normalized (a) absorbance and (b) fluorescence (370 nm excitation) spectra, (c) H_2S generation rates, and (d) biexponentially fitted time resolved photoluminescence decay curves (287 nm excitation, 530 nm detection) for non-enzymatic CdS QD synthesis under nominal solutions compositions of 0.5 mM CdAc:10 mM cysteine:1 mM PLP:10 μM $FeCl_3$ in PBS (pH 8) buffer following incubation at 70 °C (1 h), 50 °C (4 h), 40 °C (8 h), and 30 °C (24 h; H_2S rates only) and subsequent ethanol wash. H_2S generation rates were measured in the absence of CdAc.

unchanging absorbance and fluorescence spectra over the course of 2 weeks (Figure S2).

The representative HAADF-STEM images of particles resulting from 15 min (Figure 3a) and 60 min (Figure 3b) incubation reveal their clearly crystalline nature. Coalescence of single-crystal particles occurs upon QD deposition from aqueous solutions onto the holey carbon TEM grids. The CdS particles resulting from 60 min incubation have a mean size of *ca.* 3.0 ± 0.6 nm (Figure 3c), which is larger than CdS particles synthesized through enzymatic biomineralization at temperatures of 37 °C and comparable H_2S generation rates (2.1 ± 0.5 nm),[21] likely reflective of faster growth rates at the higher temperature. We have employed careful lattice indexing of images of representative particles to identify corresponding crystal structures since limited sample size and peak broadening confound conclusive alternative analysis by X-ray diffraction. The interplanar spacing and angles from images of individual particles (Figure 3d,e) match the [100] zone axis of the wurtzite-type CdS structure (Table S3) and the [101] zone axis of the zinc blende-type CdS structure (Table S4), respectively. Both of these CdS polymorphs are commonly observed to co-exist in samples derived from enzymatic, low-temperature biomineralization processes.[32]

A representative XEDS spectrum (Figure 3f) shows distinct elemental peaks for cadmium and sulfur and only a trace amount of Fe despite the use of Fe^{3+} as a catalyst in the biochemical cycle exploited here. In fact, the trace Fe signal is consistent with the background associated with the microscope (Figure S3 and Table S5), which also includes chromium (Cr), cobalt (Co), and aluminum (Al). The observed phosphorus (P) signal derives from the PBS synthesis buffer. In addition to the CdS particles appearing to be iron-free, discrete iron oxide precipitates were only very rarely observed in the sample incubated for 60 min, underscoring the robustness of the non-enzymatic PLP and Fe^{3+} catalytic system for sustainable CdS QD synthesis.

Temperature Effects on Aqueous QD Synthesis from Non-enzymatic Biochemical H_2S. The successful exploitation of the non-enzymatic biochemical cycle for CdS synthesis at the nominal 70 °C, well below the hydrothermal conditions common to conventional QD synthesis, also highlights the sustainability of this approach. To understand the potential to further reduce the synthetic energy footprint of the non-enzymatic process, we have separately evaluated the sensitivity of the H_2S production kinetics, and thus feasibility of CdS QD synthesis, at lower temperatures. Figure 4a,b compares the absorbance and fluorescence emission measured for the

https://doi.org/10.1021/acsanm.3c00805
ACS Appl. Nano Mater. 2023, 6, 7668−7678

Table 1. Average Fluorescence Lifetimes, τ_{avg}, Obtained from Fitting of Biexponential TCSPC Decay Curves Collected for Samples Synthesized Non-enzymatically and Enzymatically at Specified Temperatures

synthesis method	T [°C]	incubation time [h]	T_1 [ns]	T_2 [ns]	χ^2	B_1 [%]	τ_{avg} [ns]
non-enzymatic (this work)	70	1	1.9	25.3	1.10	13.4 ± 0.6	25.0 ± 0.6
	50	4	1.6	18.4	1.13	13.0 ± 1.1	18.2 ± 0.8
	40	8	1.2	10.6	1.12	25.8 ± 5.1	10.3 ± 2.2
enzymatic[42]	37	4	1.4	14.0	1.09	87.7	8.7

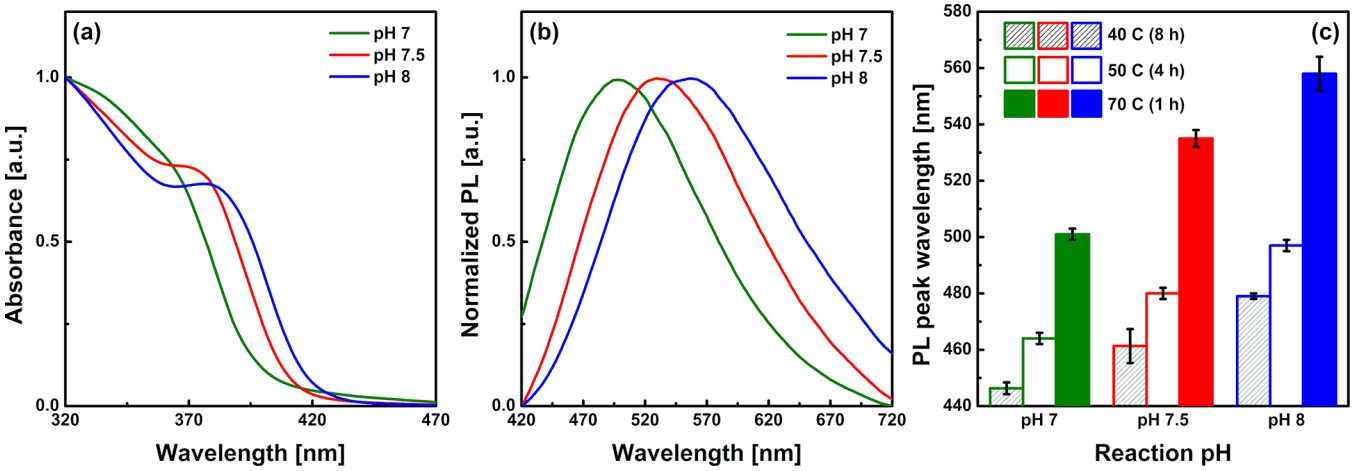

Figure 5. Normalized (a) absorbance and (b) photoluminescence (PL; 370 nm excitation) spectra of nominal solutions of 0.5 mM CdAc:10 mM cysteine:1 mM PLP:10 μM $FeCl_3$ in PBS buffers of pH 7, 7.5, and 8 following incubation at 70 °C for 1 h and subsequent ethanol wash. (c) Sensitivity of the peak PL wavelength to pH for solutions of comparable composition and pH incubated at 40 °C for 8 h, 50 °C for 4 h, or 70 °C for 1 h.

nominal solution composition upon systematic reduction of the incubation temperature toward "greener" physiological conditions employed for single-enzyme QD biomineralization. Whereas distinct absorbance bands, indicative of CdS QD synthesis, are not apparent at the lower temperatures and for the synthesis times explored here, signature CdS QD photoluminescence is measured. While CdS QDs can be detected within 15 min under the nominal synthesis conditions (70 °C) (Figure 2), photoluminescence appears only after *ca.* 4 h incubation at 50 °C and *ca.* 8 h incubation at 40 °C. Further reduction of the synthesis temperature to 30 °C results in no detectable absorbance or fluorescence even after extended 24 h incubation.

The clear blue shift of the 40 and 50 °C samples relative to the photoluminescence from the CdS particles synthesized at 70 °C is consistent with growth of larger particles at higher temperatures as confirmed by comparison of the HAADF-STEM images and corresponding particle size distributions of CdS particles resulting from 40 and 50 °C synthesis (Figure S4) with those synthesized at 70 °C (Figure 3c). We attribute the temperature sensitivity of CdS QD synthesis, at least in part, to the concomitant changes in the kinetics of the H_2S biochemistry. Figure 4c shows the temperature-dependent rates of H_2S generation in PBS (pH 8) solutions containing all components of the non-enzymatic H_2S-generating biochemical cycle (Scheme 1): cysteine, PLP, and $FeCl_3$. Despite the shorter overall incubation time, the marked increase in H_2S production rate upon increasing the synthesis temperature to 70 °C trends with the increasing particle size. The estimated activation energy for the non-enzymatic Fe^{3+}/PLP-catalyzed H_2S production (52.9 kJ/mol, Figure S5) is comparable to the characteristic activation energies for nominal enzymatic production of H_2S by sulfite reduction (*ca.* 14.1−67.0 kJ/mol).[41] The synthesis temperature likely also impacts the kinetics of nucleation and growth, but detailed study of those effects is beyond the scope of this work.

Time-correlated photoluminescence lifetime measurements for CdS QDs, synthesized non-enzymatically at various temperatures and incubation times, are shown in Figure 4d along with their biexponential fits. The resulting photoluminescence lifetime, τ_{avg}, and fast-decay parameter, B_1, offer insights into the relative structure and optical character of the QDs as a function of non-enzymatic synthesis temperature. The fast decay component is attributable to nonradiative recombination deriving from surface defects, whereas the slow decay is related to radiative recombination within the bulk crystal volume. Table 1 shows the τ_{avg} and B_1 values measured for the non-enzymatic products and draws comparison to previously reported CdS QDs synthesized via single-enzyme-based biomineralization under physiological conditions.[42]

The average fluorescence lifetime decreases by *ca.* 58% as the temperature of non-enzymatic synthesis is lowered from 70 to 40 °C, approaching the average lifetime that we have reported previously for enzymatically biomineralized CdS QDs.[42] The decreasing fluorescence lifetime upon decreasing non-enzymatic synthesis temperature (70 to 40 °C) is accompanied by an apparent increase in contributions of non-radiative surface defect-derived recombination over volumetric radiative recombination as indicated by B_1. Whereas the contributions of surface defects nearly double, the surface-to-volume ratio only increases by *ca.* 20% owing to the concomitant decrease in particle size from *ca.* 3.0 nm (70 °C, Figure 3c) to 2.6 nm (40 °C, Figure S4b). Thus, the contribution of surface defects with synthesis temperature cannot be explained simply based on surface-to-volume

https://doi.org/10.1021/acsanm.3c00805
ACS Appl. Nano Mater. 2023, 6, 7668−7678

arguments, pointing instead to the existence of intrinsic links between product quality and synthesis temperature within the framework of non-enzymatic QD synthesis. Moreover, the associated surface defect-derived recombination interestingly appears to contribute *ca.* 70% less to fluorescence decay in the case of the non-enzymatic CdS QDs than in the case of the biomineralized product. These findings collectively underscore the product quality improvement achievable with the non-enzymatic route relative to enzymatic biomineralization upon elimination of the enzyme in favor of Fe- and PLP-catalyzed H_2S generation and concomitant relaxation of temperature constraints. Unraveling the temperature and composition effects, and thereby the fundamental origin of the differences between the non-enzymatic and enzymatic processes, will be explored in future work.

Effects of pH on Non-enzymatic H_2S Biochemistry and CdS QD Optical Properties. As with temperature, the elimination of the enzyme relaxes limitations on the viable range of pH conditions that can be employed for CdS synthesis, offering additional control over system stability beyond what is possible under biomineralization conditions. Figure 5a,b shows the response of the absorbance and photoluminescence, respectively, to modest changes in synthesis pH for the nominal concentrations of CdAc, cysteine, PLP, and $FeCl_3$ following incubation at 70 °C for 1 h. A decrease in reaction pH from pH 8 (nominal) to pH 7.5 and 7 leads to a blue shift of the absorbance and photoluminescence spectra of the resulting particles. Such a blue shift in the case of CdS particles—over a pH range in which cysteine capping is expected to be relatively unaffected[43,44]—is a signature of decreasing particle size.

This decrease in particle size with decreasing pH can be attributed, at least in part, to the concomitant shift in the H_2S dissociation equilibrium away from the reactive HS^- speciation toward less reactive H_2S[45] as well as to other possible factors, including the potential for increased metal precursor hydrolysis upon pH reduction.[40,46] As shown in Figure 5c, this trend with pH persists at lower synthesis temperatures (*i.e.*, 40 and 50 °C) as well, underscoring the combined utility of temperature and pH as complementary handles, available within the non-enzymatic H_2S system, for tailoring the size, and, therefore, optical properties of CdS QDs.

Robustness of Non-enzymatic H_2S Biochemistry for Tuning CdS QD Optical Properties. To gain insights into the breadth of parameter space in which non-enzymatic aqueous Fe^{3+}/PLP-catalyzed production of H_2S for CdS QD synthesis is possible, and thereby, the robustness and range of optical properties that are accessible therein, we have applied Taguchi L9 orthogonal array-based design of experiments[47] to identify a set of nine samples comprising combinations of three concentrations (*i.e.*, levels) of each of four reagents (*i.e.*, factors): cadmium acetate, L-cysteine, PLP, and iron chloride. The specific compositional combinations that we have studied are tabulated in Table S6 along with an indication of the stability of the solutions immediately after preparation as determined by the absence of precipitate formation (Figure S6). While the majority of the solutions are stable under all three pH conditions studied, several display pH-dependent stability, which we attribute to the formation of various Cd–cysteine complexes at different Cd-to-cysteine ratios and also pH-dependent chelation strength.[48] Other complexes formed between PLP and cysteine[25] as well as $FeCl_3$ and cysteine[49] likely also contribute to the solution stability.

The absorbance and fluorescence emission measurements for solutions that bear indications of successful CdS QD synthesis at 70 °C are shown in Figure S7. Ultimately, we have chosen the presence (or absence) of fluorescence emission as an indication of successful (or unsuccessful) CdS synthesis, employing PL peak wavelength as a quantitative measure of the resulting optical character. Figure 6 shows the PL peak

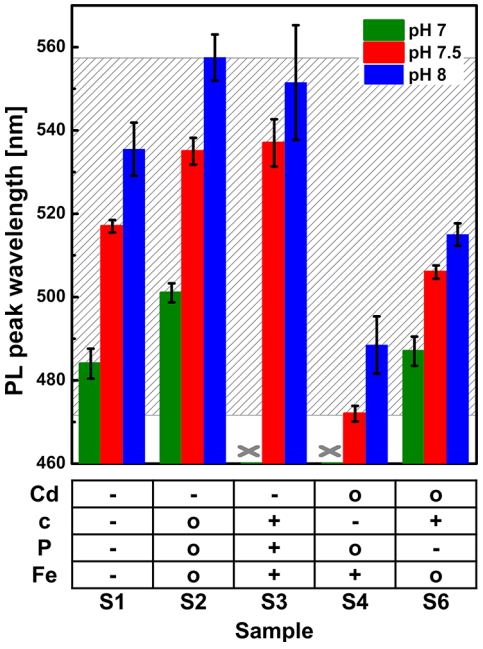

Figure 6. Sensitivity of PL peak wavelength (370 nm excitation) to four-factor experimental design at 70 °C for samples (S1–S4, S6; Table S6) containing low (−), medium (o), and high (+) concentrations of CdAc (Cd), cysteine (c), PLP (P), and $FeCl_3$. The shaded region depicts the range of PL peak wavelengths, indicative of particle size, that can be accessed under the incubation conditions.

wavelengths measured for stable synthesis solutions according to the specified sample composition and pH. Solution compositions leading to no fluorescence, and hence, undetectable CdS production, are indicated by an "X" or excluded altogether in cases where CdS QD synthesis was undetectable for a given composition for all pH conditions studied.

Most of the samples incubated at 70 °C for 1 h result in distinct absorbance and fluorescence emission spectra. As observed for the nominal (S2) synthesis conditions (Figure 5c), the data show a persistent red shift of the PL peak wavelength with increasing pH for all compositions studied. More generally, Figure 6 clearly underscores the broad composition- and pH-based tunability of the fluorescence emission peak wavelength, over *ca.* 88 ± 6 nm, under 70 °C reaction conditions. Similar compositional analysis carried out for lower-temperature synthesis at 50 °C (4 h) (Figure S8) shows persistent pH- and composition-derived tunability of the photoluminescence (Figure S9), albeit more limited in breadth (*i.e.*, by *ca.* 62%) than at 70 °C. We attribute the reduction in tunability and the more common lack of a detectable photoluminescent product at the lower synthesis temperature to the lower rates of H_2S generation. Indeed, Figure S10 shows how clear absorbance bands and strong photoluminescence signatures emerge upon extension of the 50 °C incubation to

https://doi.org/10.1021/acsanm.3c00805
ACS Appl. Nano Mater. 2023, 6, 7668–7678

24 h for compositions that initially yield no detectable product after the nominal 4 h synthesis. Ultimately, the overall robustness of the non-enzymatic Fe^{3+}/PLP-catalyzed H_2S biochemical cycle establishes a diverse set of synthetic handles—reagent composition, synthesis temperature, pH, and incubation time—that can be easily adjusted for high-resolution control over aqueous CdS QD synthesis.

CONCLUSIONS

Enzymatic routes to H_2S by turnover of sulfur-containing amino acids are key metabolic processes, which have been extensively leveraged under laboratory conditions for the "green" aqueous biomineralization of a wide range of metal sulfide QDs. Herein, we have drawn inspiration from a secondary, previously unexploited, non-enzymatic route to H_2S, demonstrating the feasibility of harnessing the associated biochemical cycle, tailoring its kinetics, and tuning system stability to be able to synthesize size tunable QDs under all-aqueous conditions as demonstrated for CdS QDs. The power of the non-enzymatic process elucidated in this work specifically for QD synthesis derives explicitly from its circumvention of classic challenges associated with enzyme activity that narrowly restrict feasible synthesis temperature and pH to physiological conditions. By stripping these limits from aqueous QD synthesis, we have shown how broader temperature and pH tunability can be exploited to boost and precisely tailor kinetics of the non-enzymatic process to produce sufficient levels of H_2S to support QD nucleation and growth over time scales of minutes to hours. Boosting QD concentrations for the scalable synthesis of optoelectronic particles suitable for applications spanning H_2 photocatalysis to solar cell sensitization, among others, would likely require careful tuning of the synthesis solution composition to realize specific product particle size while ensuring particle stability especially given the interplay between reagents, H_2S generation rate, capping, etc. revealed in this work. Yet, the number of handles for controlling particle nucleation and growth, including temperature, pH, composition, and time, and the apparent robustness of the chemistry help establish the versatility and promise of the non-enzymatic aqueous process as a powerful platform for the sustainable synthesis of a wide range of sulfur-containing materials for optoelectronic applications.

ASSOCIATED CONTENT

Supporting Information

The Supporting Information is available free of charge at https://pubs.acs.org/doi/10.1021/acsanm.3c00805.

Concentrations of photoluminescent particles as a function of nominal synthesis composition; photoluminescence evolution relative to the rate of H_2S production; H_2S production rates as a function of nominal synthesis composition; long-term stability of ethanol-washed CdS QDs; indexing of wurtzite and zinc blende structures of CdS; HAADF-STEM image of FeO_x agglomerates and XEDS-based analysis of Fe instrument background; HAADF-STEM images and corresponding particle size distributions for low-temperature non-enzymatically synthesized CdS; Arrhenius-derived activation energy for non-enzymatic H_2S generation; analysis of time-correlated photoluminescence decay; Taguchi-derived synthesis compositions along with corresponding absorbance and photoluminescence spectra of stable QD products; and UV−vis absorbance and photoluminescence of CdS QDs synthesized for 24 h at 50 °C (PDF)

AUTHOR INFORMATION

Corresponding Author

Mark A. Snyder − *Department of Chemical and Biomolecular Engineering, Lehigh University, Bethlehem, Pennsylvania 18015, United States;* orcid.org/0000-0002-8925-0588; Email: snyder@lehigh.edu

Authors

Nur Koncuy Ozdemir − *Department of Chemical and Biomolecular Engineering, Lehigh University, Bethlehem, Pennsylvania 18015, United States*

Joseph P. Cline − *Department of Materials Science and Engineering, Lehigh University, Bethlehem, Pennsylvania 18015, United States*

Tsung-Han Wu − *Department of Chemical and Biomolecular Engineering, Lehigh University, Bethlehem, Pennsylvania 18015, United States*

Leah C. Spangler − *Department of Chemical and Life Science Engineering, Virginia Commonwealth University, Richmond, Virginia 23284, United States*

Steven McIntosh − *Department of Chemical and Biomolecular Engineering, Lehigh University, Bethlehem, Pennsylvania 18015, United States;* orcid.org/0000-0003-4664-2028

Christopher J. Kiely − *Department of Chemical and Biomolecular Engineering and Department of Materials Science and Engineering, Lehigh University, Bethlehem, Pennsylvania 18015, United States*

Complete contact information is available at: https://pubs.acs.org/10.1021/acsanm.3c00805

Notes

The authors declare no competing financial interest.

ACKNOWLEDGMENTS

The authors gratefully acknowledge support for this work from the National Science Foundation through the SNM-IS program under grant numbers CBET-1727166 and CBET-1821389.

REFERENCES

(1) Liu, Y.; Li, Y.; Kang, H.; Jin, T.; Jiao, L. Design, Synthesis, and Energy-Related Applications of Metal Sulfides. *Mater. Horiz.* **2016**, *3*, 402−421.

(2) Tomboc, G. M.; Gadisa, B. T.; Joo, J.; Kim, H.; Lee, K. Hollow Structured Metal Sulfides for Photocatalytic Hydrogen Generation. *ChemNanoMat* **2020**, *6*, 850−869.

(3) Tsuji, I.; Kato, H.; Kobayashi, H.; Kudo, A. Photocatalytic H_2 Evolution Reaction from Aqueous Solutions over Band Structure-Controlled $(AgIn)_xZn_{2(1-x)}S_2$ Solid Solution Photocatalysts with Visible-Light Response and Their Surface Nanostructures. *J. Am. Chem. Soc.* **2004**, *126*, 13406−13413.

(4) Bera, D.; Qian, L.; Tseng, T.-K. K.; Holloway, P. H. Quantum Dots and Their Multimodal Applications: A Review. *Materials* **2010**, *3*, 2260−2345.

(5) Jamieson, T.; Bakhshi, R.; Petrova, D.; Pocock, R.; Imani, M.; Seifalian, A. M. Biological Applications of Quantum Dots. *Biomaterials* **2007**, *28*, 4717−4732.

(6) Jean, J.; Xiao, J.; Nick, R.; Moody, N.; Nasilowski, M.; Bawendi, M.; Bulović, V. Synthesis Cost Dictates the Commercial Viability of Lead Sulfide and Perovskite Quantum Dot Photovoltaics. *Energy Environ. Sci.* **2018**, *11*, 2295−2305.
(7) Abe, K.; Kimura, H. The Possible Role of Hydrogen Sulfide as an Endogenous Neuromodulator. *J. Neurosci.* **1996**, *16*, 1066−1071.
(8) Kimura, H. Hydrogen Sulfide: Its Production, Release and Functions. *Amino Acids* **2011**, *41*, 113−121.
(9) Cao, X.; Ding, L.; Xie, Z.; Yang, Y.; Whiteman, M.; Moore, P. K.; Bian, J.-S. A Review of Hydrogen Sulfide Synthesis, Metabolism, and Measurement: Is Modulation of Hydrogen Sulfide a Novel Therapeutic for Cancer? *Antioxid. Redox Signaling* **2019**, *31*, 1−38.
(10) Kolluru, G. K.; Shen, X.; Bir, S. C.; Kevil, C. G. Hydrogen Sulfide Chemical Biology: Pathophysiological Roles and Detection. *Nitric Oxide* **2013**, *35*, 5−20.
(11) Jiang, Z.; Wang, B.; Yu, J. C.; Wang, J.; An, T.; Zhao, H.; Li, H.; Yuan, S.; Wong, P. K. $AgInS_2/In_2S_3$ Heterostructure Sensitization of Escherichia Coli for Sustainable Hydrogen Production. *Nano Energy* **2018**, *46*, 234−240.
(12) Dameron, C. T.; Reese, R. N.; Mehra, R. K.; Kortan, A. R.; Carroll, P. J.; Steigerwald, M. L.; Brus, L. E.; Winge, D. R. Biosynthesis of Cadmium Sulphide Quantum Semiconductor Crystallites. *Nature* **1989**, *338*, 596−597.
(13) Hulkoti, N. I.; Taranath, T. C. Biosynthesis of Nanoparticles Using Microbes—A Review. *Colloids Surf., B* **2014**, *121*, 474−483.
(14) Feng, Y.; Marusak, K. E.; You, L.; Zauscher, S. Biosynthetic Transition Metal Chalcogenide Semiconductor Nanoparticles: Progress in Synthesis, Property Control and Applications. *Curr. Opin. Colloid Interface Sci.* **2018**, *38*, 190−203.
(15) Zhao, K.; Li, H.; Li, S.; Yang, G. Regulation of Cystathionine Gamma-Lyase/H2S System and Its Pathological Implication. *Front. Biosci. (Landmark Ed)* **2014**, *19*, 1355−1369.
(16) Dunleavy, R.; Lu, L.; Kiely, C. J.; McIntosh, S.; Berger, B. W. Single-Enzyme Biomineralization of Cadmium Sulfide Nanocrystals with Controlled Optical Properties. *Proc. Natl. Acad. Sci. U. S. A.* **2016**, *113*, 5275−5280.
(17) Spangler, L. C.; Lu, L.; Kiely, C. J.; Berger, B. W.; McIntosh, S. Biomineralization of PbS and PbS-CdS Core-Shell Nanocrystals and Their Application in Quantum Dot Sensitized Solar Cells. *J. Mater. Chem. A* **2016**, *4*, 6107−6115.
(18) Ozdemir, N. K.; Cline, J. P.; Kiely, C. J.; McIntosh, S.; Snyder, M. A. Scalable Biomineralization of CdS Quantum Dots by Immobilized Cystathionine γ-Lyase. *ACS Sustainable Chem. Eng.* **2020**, *8*, 15189−15198.
(19) Spangler, L. C.; Chu, R.; Lu, L.; Kiely, C. J.; Berger, B. W.; McIntosh, S. Enzymatic Biomineralization of Biocompatible $CuInS_2$, $(CuInZn)S_2$ and $CuInS_2$/ZnS Core/Shell Nanocrystals for Bioimaging. *Nanoscale* **2017**, *9*, 9340−9351.
(20) Sadeghnejad, A.; Lu, L.; Cline, J.; Ozdemir, N. K.; Snyder, M. A.; Kiely, C. J.; McIntosh, S. In Situ Biomineralization of $Cu_xZn_ySn_zS_4$ Nanocrystals within TiO_2-Based Quantum Dot Sensitized Solar Cell Anodes. *ACS Appl. Mater. Interfaces* **2019**, *11*, 45656−45664.
(21) Spangler, L. C.; Cline, J. P.; Kiely, C. J.; McIntosh, S. Low Temperature Aqueous Synthesis of Size-Controlled Nanocrystals through Size Focusing: A Quantum Dot Biomineralization Case Study. *Nanoscale* **2018**, *10*, 20785−20795.
(22) Chiku, T.; Padovani, D.; Zhu, W.; Singh, S.; Vitvitsky, V.; Banerjee, R. H_2S Biogenesis by Human Cystathionine γ-Lyase Leads to the Novel Sulfur Metabolites Lanthionine and Homolanthionine and Is Responsive to the Grade of Hyperhomocysteinemia. *J. Biol. Chem.* **2009**, *284*, 11601−11612.
(23) Yamagata, S.; Isaji, M.; Yamane, T.; Iwama, T. Substrate Inhibition of L-Cysteine α,β-Elimination Reaction Catalyzed by L-Cystathionine γ-Lyase of Saccharomyce Cerevisiae. *Biosci., Biotechnol., Biochem.* **2002**, *66*, 2706−2709.
(24) El-Sayed, A. S. A.; Yassin, M. A.; Khalaf, S. A.; El-Batrik, M.; Ali, G. S.; Esener, S. Biochemical and Pharmacokinetic Properties of PEGylated Cystathionine γ-Lyase from Aspergillus Carneus KF723837. *J. Mol. Microbiol. Biotechnol.* **2015**, *25*, 301−310.
(25) Yang, J.; Minkler, P.; Grove, D.; Wang, R.; Willard, B.; Dweik, R.; Hine, C. Non-Enzymatic Hydrogen Sulfide Production from Cysteine in Blood Is Catalyzed by Iron and Vitamin B6. *Commun. Biol.* **2019**, *2*, 194.
(26) Asimakopoulou, A.; Panopoulos, P.; Chasapis, C. T.; Coletta, C.; Zhou, Z.; Cirino, G.; Giannis, A.; Szabo, C.; Spyroulias, G. A.; Papapetropoulos, A. Selectivity of Commonly Used Pharmacological Inhibitors for Cystathionine β Synthase (CBS) and Cystathionine γ Lyase (CSE). *Br. J. Pharmacol.* **2013**, *169*, 922−932.
(27) Jing, L.; Kershaw, S. V.; Li, Y.; Huang, X.; Li, Y.; Rogach, A. L.; Gao, M. Aqueous Based Semiconductor Nanocrystals. *Chem. Rev.* **2016**, *116*, 10623−10730.
(28) Gruenwedel, D. W.; Patnaik, R. K. Release of Hydrogen Sulfide and Methyl Mercaptan from Sulfur-Containing Amino Acids. *J. Agric. Food Chem.* **1971**, *19*, 775−779.
(29) ATWATER, R. What the Institutional Buyer Wishes to Know about Canned Foods*. *J. Am. Diet. Assoc.* **1930**, *5*, 299−303.
(30) Lim, H.; Woo, J. Y.; Lee, D. C.; Lee, J.; Jeong, S.; Kim, D. Continuous Purification of Colloidal Quantum Dots in Large-Scale Using Porous Electrodes in Flow Channel. *Sci. Rep.* **2017**, *7*, 43581.
(31) Taguchi, G. Off-Line and on-Line Quality Control Systems. In *Proceedings of the International Conference on Quality Control*; Japan Tokyo, 1978; Vol. *4*, pp. 1−5.
(32) Yang, Z.; Lu, L.; Berard, V. F.; He, Q.; Kiely, C. J.; Berger, B. W.; McIntosh, S. Biomanufacturing of CdS Quantum Dots. *Green Chem.* **2015**, *17*, 3775−3782.
(33) Yang, Z.; Lu, L.; Kiely, C. J.; Berger, B. W.; McIntosh, S. Biomineralized CdS Quantum Dot Nanocrystals: Optimizing Synthesis Conditions and Improving Functional Properties by Surface Modification. *Ind. Eng. Chem. Res.* **2016**, *55*, 11235−11244.
(34) Matsuo, Y. Formation of Schiff Bases of Pyridoxal Phosphate. Reaction with Metal Ions1. *J. Am. Chem. Soc.* **1957**, *79*, 2011−2015.
(35) Upadhyay, Y.; Bothra, S.; Kumar, R.; Kumar, S. K.; Sahoo, S. K. Mimicking Biological Process to Detect Alkaline Phosphatase Activity Using the Vitamin B6 Cofactor Conjugated Bovine Serum Albumin Capped CdS Quantum Dots. *Colloids Surf., B* **2020**, *185*, No. 110624.
(36) Yadav, A.; Upadhyay, Y.; Bera, R. K.; Sahoo, S. K. Vitamin B6 Cofactors Guided Highly Selective Fluorescent Turn-on Sensing of Histamine Using Beta-Cyclodextrin Stabilized ZnO Quantum Dots. *Food Chem.* **2020**, *320*, No. 126611.
(37) Bhardwaj, V.; Bothra, S.; Upadhyay, Y.; Sahoo, S. K. Cascade Detection of Pyridoxal 5′-Phosphate and Al3+ Ions Based on Dual-Functionalized Red-Emitting Copper Nanoclusters. *ACS Appl. Nano Mater.* **2021**, *4*, 6231−6238.
(38) Alqarni, A. O.; Alkahtani, S. A.; Mahmoud, A. M.; El-Wekil, M. M. Design of "Turn On" Fluorometric Nanoprobe Based on Nitrogen Doped Graphene Quantum Dots Modified with β-Cyclodextrin and Vitamin B6 Cofactor for Selective Sensing of Dopamine in Human Serum. *Spectrochim. Acta, Part A* **2021**, *248*, No. 119180.
(39) Swinehart, D. F. The Beer-Lambert Law. *J. Chem. Educ.* **1962**, *39*, 333.
(40) Zhang, H.; Chen, B.; Banfield, J. F. Particle Size and PH Effects on Nanoparticle Dissolution. *J. Phys. Chem. C* **2010**, *114*, 14876−14884.
(41) Nowak, A.; Kusewicz, D.; Kalinowska, H.; Turkiewicz, M.; Patelski, P. Production of H2S and Properties of Sulfite Reductase from Selected Strains of Wine-Producing Yeasts. *Eur. Food Res. Technol.* **2004**, *219*, 84−89.
(42) Sakizadeh, J.; Cline, J. P.; Snyder, M. A.; Kiely, C. J.; McIntosh, S. Biomineralization of Nanocrystalline CdS/ZnS Photocatalysts via Controlled Surface Passivation for Enhanced Hydrogen Evolution. *ACS Appl. Nano Mater.* **2022**, *5*, 2293−2304.
(43) Cai, Z.-X.; Yang, H.; Zhang, Y.; Yan, X.-P. Preparation, Characterization and Evaluation of Water-Soluble l-Cysteine-Capped-CdS Nanoparticles as Fluorescence Probe for Detection of Hg(II) in Aqueous Solution. *Anal. Chim. Acta* **2006**, *559*, 234−239.
(44) Bae, W.; Abdullah, R.; Mehra, R. K. Cysteine-Mediated Synthesis of CdS Bionanocrystallites. *Chemosphere* **1998**, *37*, 363−385.

https://doi.org/10.1021/acsanm.3c00805
ACS Appl. Nano Mater. 2023, 6, 7668−7678

(45) Yongsiri, C.; Vollertsen, J.; Hvitved-Jacobsen, T. Effect of Temperature on Air-Water Transfer of Hydrogen Sulfide. *J. Environ. Eng.* **2004**, *130*, 104−109.
(46) Winter, J. O.; Gomez, N.; Gatzert, S.; Schmidt, C. E.; Korgel, B. A. Variation of Cadmium Sulfide Nanoparticle Size and Photoluminescence Intensity with Altered Aqueous Synthesis Conditions. *Colloids Surf., A* **2005**, *254*, 147−157.
(47) Davis, R. *Application of Taguchi-Based Design of Experiments for Industrial Chemical Processes*; Silva, P. J. E.-V., Ed.; IntechOpen: Rijeka, 2018; p Ch. 9, DOI: 10.5772/intechopen.69501.
(48) Jalilehvand, F.; Leung, B. O.; Mah, V. Cadmium(II) Complex Formation with Cysteine and Penicillamine. *Inorg. Chem.* **2009**, *48*, 5758−5771.
(49) Bhattacharyya, A.; Stavitski, E.; Dvorak, J.; Martínez, C. E. Redox Interactions between Fe and Cysteine: Spectroscopic Studies and Multiplet Calculations. *Geochim. Cosmochim. Acta* **2013**, *122*, 89−100.

https://doi.org/10.1021/acsanm.3c00805
ACS Appl. Nano Mater. 2023, 6, 7668−7678